REPORT DOCUMENTATION PAGE

Form Approved OMB NO. 0704-0188

1. REPORT DATE (DD-MM-YYYY)	2. REPORT TYPE	3. DATES COVERED (From - To)
29-09-2022	Final Report	8-Jan-2021 - 31-Jan-2022

4. TITLE AND SUBTITLE
Final Report: In-Situ Micro-Mechanical System for Testing of Advanced Materials under Extreme Conditions of Temperature, Strain-Rate and Applied Stress

5a. CONTRACT NUMBER
W911NF-21-1-0042

5b. GRANT NUMBER

5c. PROGRAM ELEMENT NUMBER
611103

5d. PROJECT NUMBER

5e. TASK NUMBER

5f. WORK UNIT NUMBER

6. AUTHORS

7. PERFORMING ORGANIZATION NAMES AND ADDRESSES
Iowa State University of Science and Techn
1138 Pearson Hall
505 Morrill Road
Ames, IA 50011 -2103

8. PERFORMING ORGANIZATION REPORT NUMBER

9. SPONSORING/MONITORING AGENCY NAME(S) AND ADDRESS (ES)
U.S. Army Research Office
P.O. Box 12211
Research Triangle Park, NC 27709-2211

10. SPONSOR/MONITOR'S ACRONYM(S)
ARO

11. SPONSOR/MONITOR'S REPORT NUMBER(S)
77460-TE-RIP.1

12. DISTRIBUTION AVAILIBILITY STATEMENT
Approved for public release; distribution is unlimited.

13. SUPPLEMENTARY NOTES
The views, opinions and/or findings contained in this report are those of the author(s) and should not contrued as an official Department of the Army position, policy or decision, unless so designated by other documentation.

14. ABSTRACT

15. SUBJECT TERMS

16. SECURITY CLASSIFICATION OF:			17. LIMITATION OF ABSTRACT	15. NUMBER OF PAGES	19a. NAME OF RESPONSIBLE PERSON
a. REPORT	b. ABSTRACT	c. THIS PAGE			Siddhartha Pathak
UU	UU	UU	UU		19b. TELEPHONE NUMBER 515-294-9280

Standard Form 298 (Rev 8/98)
Prescribed by ANSI Std. Z39.18

RPPR Final Report
as of 29-Sep-2022

Agency Code: 21XD

Proposal Number: 77460TERIP
Agreement Number: W911NF-21-1-0042

INVESTIGATOR(S):

Name: Siddhartha Pathak
Email: pathak@iastate.edu
Phone Number: 5152949280
Principal: Y

Organization: **Iowa State University of Science and Technology**
Address: 1138 Pearson Hall, Ames, IA 500112103
Country: USA
DUNS Number: 005309844
EIN: 426004224
Report Date: 30-Apr-2022
Date Received: 29-Sep-2022
Final Report for Period Beginning 08-Jan-2021 and Ending 31-Jan-2022
Title: In-Situ Micro-Mechanical System for Testing of Advanced Materials under Extreme Conditions of Temperature, Strain-Rate and Applied Stress
Begin Performance Period: 08-Jan-2021
End Performance Period: 31-Jan-2022
Report Term: 0-Other
Submitted By: Siddhartha Pathak
Email: pathak@iastate.edu
Phone: (515) 294-9280
Distribution Statement: 1-Approved for public release; distribution is unlimited.

STEM Degrees: 2
STEM Participants: 5

Major Goals: This DURIP grant provided support for expanding the capabilities of the Alemnis in-situ micro-mechanical system to include extreme conditions of temperature (-150 to 1000 C), a wide range of applied strain-rates (10^-4 to 10^4/s) and high applied stresses. In the current materials and mechanical research environment, mechanical properties of microscale volume are traditionally studied using indentation tests which are conducted at quasistatic rates (i.e. strain rates in the range of 10^-5 to 10^-2 /s) and under ambient conditions (s room temperature). However, the dynamic properties of the local regions of interest remain unexplored, especially at elevated/cryogenic temperatures and applied stresses. With the newly expanding capabilities of our current Alemnis in-situ SEM system we have been able to evaluate the local material response over wide extremes of temperature, strain rates and loading conditions.

The DURIP award provided a number of upgrades to our existing Alemnis Standard Assembly (ASA) manufactured by Alemnis AG in order to enhance its capabilities for testing under extreme conditions. Micro-mechanical tests are moving beyond the basic measurement of hardness and elastic modulus to encompass a host of different mechanical properties such as strain rate sensitivity, stress relaxation, creep, and fracture toughness by taking advantage of focused ion beam (FIB) milled sample geometries (e.g., micropillars, micro-tensile geometries, beams, etc.) and additively manufactured (AM) microstructures. New developments, such as high strain rate and high and low-temperature tests, are needed to extend the range of properties that can be studied at the micro and nanoscale. However, such techniques are challenging due to low oscillation frequencies, long duration of tests, and significant thermal drift when attempted with standard indentation instruments. Therefore such capabilities are scarce within the US as well as internationally.

Specifically, the DURIP award provided funds to purchase the following upgrades:

1. LTM-CRYO (Low-Temperature Module). Upgrade of existing capabilities to -150 C

2. HTM (High-Temperature Module). Upgrade of existing capabilities to 1000 C

The primary advantage of the upgraded module will be that it can now cover such an extensive range of temperatures from (-150 C up to 1000 C) and strain rates (10^-4 to 10^4/s). These upgrades allow us the unique ability to measure activation energies and volumes from these tests, and hence ascertain the operative deformation mechanisms at these local length scales.

- These upgrades will allow variable strain rate testing to be performed over the broadest range of temperature and on an extensive range of sample geometries (flat, curved, micropillar, microbeam, etc.).

- Tip and sample temperatures can be controlled separately, and it allows us to avoid any thermal drift (<10nm/min at 600 C).

- The modular and robust design allows easy exchange of the heaters and indenters by the user. All indenter shapes and materials are available.

- Cryo setup will be essential to explore materials behavior at low temperatures, for example, in investigations of ductile to brittle transition temperature concept in a broad range of materials.

- Flexible to be used in conjunction with numerous other analytical instruments like AFM, SEM, and X-ray diffraction systems.

- All the experiments can be done in compression as well as in tension modes.

- This is a unique combination of a wide variety of testing capabilities, which will be the first of its kind in the US in any university or a US national laboratory.

Accomplishments: All of the project goals were accomplished. Specifically, the funds from the DURIP award were used to purchase the following upgrades, which were installed by the vendor during the project period:

1. LTM-CRYO (Low-Temperature Module). Upgrade of existing capabilities to -150 C

2. HTM (High-Temperature Module). Upgrade of existing capabilities to 1000 C

Results from theses upgrades are described in the ‘Upload’ section of this report.

Training Opportunities: The following training opportunities were offered on the Alemnis Nanoindenter:

• Basic training was given to staff and safety coordinators at Iowa State University

• Advanced training was given to graduate student Skye Supakul to perform ultra-high strain rate, ultra-high temperature, and low temperature (cryo) nanomechanical testing by Alemnis application specialist Simeon Bodenmann

• Advanced training was given to graduate student Deeksha Kodangal to perform low temperature (cryo) nanomechanical testing by Skye Supakul

• Advanced training was given to graduate student Manish Kumar to perform low temperature (cryo) nanomechanical testing by Skye Supakul

• Basic training was given to graduate student Landon Hickman to perform simple micromechanical testing by Skye Supakul

Results Dissemination: Conference/Professional Presentations

• Manish Kumar, Sid Pathak “Structure and Properties of Solder Joints Produced in Microgravity and Terrestrial Conditions” 2022 International Space Station Research and Development Conference (ISSRDC-2022), Washington DC, Maryland, USA

• S. Pathak, S. Supakul, ‘Mechanistic Design of Metal/MAX Multilayered Nanolaminates for Tunable Strength and Toughness’, 2022 DEPSCOR DOD Day, University of South Dakota

• S. Pathak, S. Supakul, ‘In-Situ Micro-Mechanical System for Testing of Advanced Materials Under Extreme Conditions of Temperature, Strain-Rate and Applied Stress’, 2022 DEPSCOR DOD Day, University of South Dakota

• S. Supakul, S. Pathak, ‘Mechanistic-Design of Multilayered Nanocomposites: Hierarchical Metal-MAX Materials for Tunable Strength and Toughness’, 2022 TMS Annual Meeting and Exhibition. (Oral Presentation)

• S. Supakul, S. Picak, S. Pathak. “In-Situ Micro-Mechanical System for Testing of Advanced Materials Under Extreme Conditions of Temperature, Strain-Rate, and Applied Stress”, 2021 Defense TechConnect, Washington DC, Maryland, USA

Honors and Awards: ThinkSwiss Scholarship 2021 – A PhD student, Ms. Soumya Varma, was the recipient of the 2021 ThinkSwiss Scholarship - awarded by the Embassy of Switzerland in the US - which allows her to travel to travel to EMPA (Laboratory for Mechanics of Materials and Nanostructures, the Swiss Federal Laboratories for Materials Science and Technology), Thun, Switzerland. This trip provided access and training on the Alemnis Nanoindenter (Alemnis is based at EMPA) required for Ms. Varma’s thesis. See Section 2.5 Micromechanical Investigations of the Remarkable Damage Tolerance in Tooth-Enamel of Hadrosaurid Dinosaurs (page 18 of the attached document)
Ms. Varma has graduated with a PhD from the Department of Materials Science and Engineering at Iowa State University in Summer 2022.

ThinkSwiss Scholarship 2022. Graduate student Syke Supakul is the recipient of the 2022 ThinkSwiss Scholarship - awarded by the Embassy of Switzerland in the US - which allows him to travel to travel to EMPA (Laboratory for Mechanics of Materials and Nanostructures, the Swiss Federal Laboratories for Materials Science and Technology), Thun, Switzerland. This trip will provide access and training on the Alemnis Nanoindenter (Alemnis is based at EMPA) and the combined Atomic Layer Deposition (ALD) Physical Vapor Deposition (PVD) deposition system, the SC-1 from Swiss Cluster.
The key features of this internship include:

o Training and intimate development on the Alemnis Nanoindenter suite of extreme temperature (-150C to 1000C) and strain rate (10^-4 /s to 10^4 /s) testing for micromechanical testing

o Training and development on the SwissCluster-1 ALD-PVD system that allows for combined ALD-PVD in one chamber without breaking vacuum

o TEM lamella fabrication and microscopy for local microstructural characterization

o STEM imaging with precession electron diffraction and electron energy loss spectroscopy for local chemical compositional analysis

o Electron backscattered diffraction for orientational information

o X-Ray diffraction for structural characterization

o X-Ray fluorescence spectroscopy and X-ray energy dispersive spectroscopy for chemical analysis

o Collaboration with various scientists and post-docs from all over the world with expertise on micromechanics, microscale materials, and thin film development.

RPPR Final Report
as of 29-Sep-2022

Protocol Activity Status:

Technology Transfer: Nothing to Report

PARTICIPANTS:

Participant Type: PD/PI
Participant: Siddhartha Pathak
Person Months Worked: 1.00 **Funding Support:**
Project Contribution:
National Academy Member: N

Participant Type: Technician
Participant: Michelle Grawe
Person Months Worked: 1.00 **Funding Support:**
Project Contribution:
National Academy Member: N

Participant Type: Technician
Participant: Matthew Lynn
Person Months Worked: 1.00 **Funding Support:**
Project Contribution:
National Academy Member: N

Participant Type: Technician
Participant: Darrel Enyart
Person Months Worked: 1.00 **Funding Support:**
Project Contribution:
National Academy Member: N

Participant Type: Graduate Student (research assistant)
Participant: Skye Nuriel Supakul
Person Months Worked: 6.00 **Funding Support:**
Project Contribution:
National Academy Member: N

Participant Type: Graduate Student (research assistant)
Participant: Deeksha Kodangal
Person Months Worked: 1.00 **Funding Support:**
Project Contribution:
National Academy Member: N

Participant Type: Graduate Student (research assistant)
Participant: Manish Kumar
Person Months Worked: 3.00 **Funding Support:**
Project Contribution:

National Academy Member: N

Participant Type: Graduate Student (research assistant)
Participant: Soumya Varma
Person Months Worked: 1.00 **Funding Support:**
Project Contribution:
National Academy Member: N

Participant Type: Graduate Student (research assistant)
Participant: Landon Hickman
Person Months Worked: 1.00 **Funding Support:**
Project Contribution:
National Academy Member: N

Partners

,

I certify that the information in the report is complete and accurate:
Signature: Siddhartha Pathak
Signature Date: 9/29/22 11:46AM

Title: In-Situ Micro-Mechanical System for Testing of Advanced Materials under Extreme Conditions of Temperature, Strain-Rate and Applied Stress

Proposal No: Army DURIP Proposal No. 77460-MS-RIP (W911NF2110042)

PI: Dr. Siddhartha (Sid) Pathak (Iowa State University)

Program Officer: Dr. Daniel P. Cole, Army Research Office

1.0 Project Summary. This DURIP grant provided support for expanding the capabilities of the Alemnis *in-situ* micro-mechanical system to include extreme conditions of temperature (-150 to 1000 ºC), a wide range of applied strain-rates (10^{-4} to 10^{4}/s) and high applied stresses. In the current materials and mechanical research environment, mechanical properties of microscale volume are traditionally studied using indentation tests which are conducted at quasistatic rates (i.e. strain rates in the range of 10^{-5} to 10^{-2} /s) and under ambient conditions (s room temperature). However, the dynamic properties of the local regions of interest remain unexplored, especially at elevated/cryogenic temperatures and applied stresses. With the newly expanding capabilities of our current Alemnis *in-situ* SEM system we have been able to evaluate the local material response over wide extremes of temperature, strain rates and loading conditions.

The Alemnis SEM system was chosen as the best combination of system performance, modular design and cost target. The instrument is specifically designed to leverage the advanced imaging capabilities of scanning electron microscopes, and integrated focused ion beam and/or electron backscatter diffraction systems, which allows us to capture the local microstructural evolution during the course of deformation. This is a unique system (and different from other manufacturers) in that it is a depth-controlled system. As mentioned earlier, most indentation systems are load controlled. Being depth controlled it will allow us to achieve high strain rate measurements from 10^{-4}/s to 10^{4}/s strain rates (thus covering an impressive 9 orders of magnitude of strain rates). Such high strain rate measurements can be used to mimic ballistic tests at the micron scale, perform strain rate jump tests, as well as measure activation energies and activation volumes from sub-micrometer sized specimens, which can be highly instrumental in understanding their deformation mechanisms especially at elevated and cryogenic temperatures. In addition to the traditional indentation mode, this instrument will also allow testing of varied loading geometries, such as micro-compression, micro-(cantilever and 3-point) bending, micro tension, low cycle fatigue, nanoscale wear tests, etc. (**Fig. 1**). No other manufacturer (US or non-US) offers this range of capabilities.

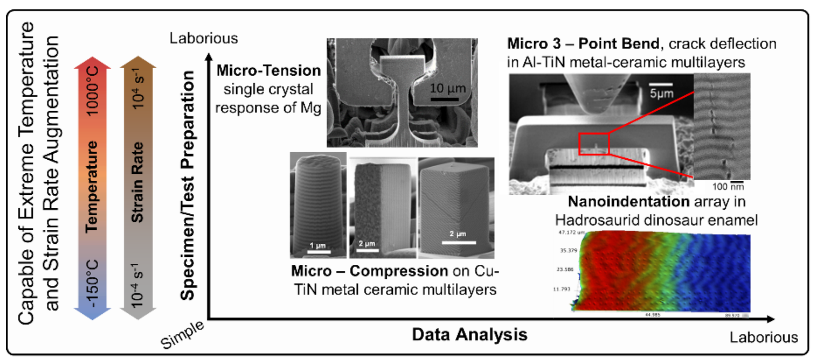

Fig 1. Overview of expanded testing capabilities of the Alemnis in-situ micro-mechanical system. Insets show FIB fabricated 3D test geometries for micro-compression, micro-tension, and micro 3 pt. bend showing crack deflection in layered composites.

1.1 Alemnis Nanoindenter Platform

The Alemnis indenter system was chosen as the best combination of system performance, modular design, and cost target. The instrument is specifically designed to leverage the advanced imaging capabilities of microscopes including both light and scanning electron microscopes and integrated FIB/SEM systems, and synchrotron x-rays. Furthermore, we highlight the following features:

True displacement mode. This is a unique system, different from other manufacturers, that utilizes a depth-controlled system. Most nanomechanical systems are load controlled, having difficulty to study fracture and stress relaxation in materials. With a depth-controlled system, precision control of the displacement allows for enhanced fracture Most important features of the Alemnis system from proposal and slide; input a table

Ultra-high strain rate. The system is equipped with unique and patented high strain rate modulus to open completely new possibilities in material science. Ultra-high strain rates (up to 10,000 s^{-1}) can be reached mimicking ballistic tests at the micron scale. Strain rate response of materials covering 9 orders of magnitude change in strain rates (10^{-4} s^{-1} to 10^{4} s^{-1}) can be studied at the micrometer length scales with the same instrument. This wide range of strain rates allows for 1) low and high cycle fatigue tests on micropillars and indentation over millions of cycles within a few minutes with oscillations frequencies of several kHz, 2) dynamic lateral force measurements in 3 axis during scratch tests for instantaneous load changes in 3 dimensions, 3) the ability to perform strain rate jump tests over a wide range of strain rates for measurements of the activation volume and energies from sub-micrometer sized specimens, and 4) viscoelasatic properties of polymers or changes in mechanical properties of multilayers and functionally graded materials as a function of indentation depths using the sinus mode indents. No other manufacturer (US or non-US) has this capability.

Extreme Temperatures. The system is equipped with cryo (-150°C) and ultra-high temperature (1000°C) modules that provide localized tip and sample cooling or heating. With the capability to cover a wide range of temperatures, a map of the mechanical properties over a wide temperature spectrum can be made. Changes in the mechanical properties of materials before, during, and after phase changes can be captured using this system. Coupled with the ultra-high strain rate capabilities, it is possible to experimentally determine the activation energy for materials at the sub-micron level.

Wide Load Range and displacement platform. Covering a wide range of loads (4 µN up to 1.5N) and displacements of 40 µm up to 100 µm, these features not only allow for measurements at shallow depths, but also capturing the deformation response for other loading geometries such as micro-pillar compression (e.g. milled using FIB or other etching techniques), micro (cantilever and 3-point) bending, micro-tension, low cycle fatigue, nanoscale wear tests, micro-lattices, and 3-d printed structures where large displacements and loads are necessary.

Specifically, the DURIP award provided funds to purchase the following upgrades:

1. LTM-CRYO (Low-Temperature Module). Upgrade of existing capabilities to -150°C

2. HTM (High-Temperature Module). Upgrade of existing capabilities to 1000°C

● These upgrades allow variable strain rate testing to be performed over the broadest range of temperature and on an extensive range of sample geometries (flat, curved, micropillar, microbeam, etc.).

● Tip and sample temperatures are now controlled separately, and it allows us to avoid any thermal drift (<10nm/min at 600°C).

● The modular and robust design allows easy exchange of the heaters and indenters by the user. All indenter shapes and materials are available.

● Cryo setup is essential to explore materials behavior at low temperatures, for example, in investigations of ductile to brittle transition temperature concept in a broad range of materials.

● Flexible to be used in conjunction with numerous other analytical instruments

2.0.0 Current Research Enhanced by Capabilities of Alemnis System. This instrument is one of the only four instruments of its kind are currently available in the Unites States [1], and a handful abroad [2-4]. It is the first of its kind at Iowa State University (ISU) as well as in the state of Iowa, which is an NSF and DOE EPSCoR (Experimental Program to Stimulate Competitive Research) designated jurisdiction. With this micro-mechanical system capable of extreme conditions we have been able to pursue research in several key areas of interest to the department of Defense, and the Army in particular, where it will significantly expand the capabilities available at local (sub-µm to nm) length scales: (1) mechanistic design of hierarchical multilayered nanocomposites for enhanced strength and toughness; (2) statistical investigation of damage formation in polycrystalline metallic materials under dynamic loading conditions; (3) additively manufactured shape memory alloys for on demand shape change and damage mitigation; (4) investigating the local stricture-property correlations in alloys for cryogenic (space) applications; and (5) biomechanics of hierarchically-structured enamel in grinding dentitions. Collectively, this work – enabled by the expanded capabilities of the Alemnis system – has advanced multidisciplinary research programs in science and engineering, which spans from structural engineering materials, energy and functional materials to nanostructured materials and natural biological materials. Additionally, this system has helped to establish a research capability that is unique in the state as well as in the entire country, thus fostering an exclusive research-related education system at courses taught at Iowa State University. The system has significantly augmented cross-disciplinary collaborations with DoD and DoE laboratories such as the Army Research Lab, Ames National Laboratory (where the PI has an affiliate position) and Los Alamos National Laboratory (where the PI is the president of the Users Executive Council), especially in the fields of micro-mechanical testing and advanced manufacturing.

Below is a brief overview of the work and progress completed on principal projects that enabled by this equipment development. These projects span across the diverse fields materials, mechanics and biology.

Table 1. *Overview of which sections are associated with the different Alemnis nanoindenter system mode/capability*

Mode/Capability	**Section(s)**
True Displacement control	2.1.2 Stress-strain response of Ti-Ti_2AlC Multilayered deposited Metal and MAX phase nanocomposites and nanolaminates (**page 6**) 2.2.3 Micro-Tension-Compression Asymmetry in Mg-Nb Multilayered Nanolaminates (**page 11**) 2.3 Fracture Studies of Cu-TiN and Al-TiN Multilayered Nanolaminates using Microcompression (**page 13**) 2.5 Micromechanical Investigations of the Remarkable Damage Tolerance in Tooth-Enamel of Hadrosaurid Dinosaurs (**page 18**)
Ultra-high strain rate	2.1.1 High Strain Rate Response of Single Crystal MAX Phase Ta_2AlC (**page 4**) 2.2.2 Combined Elevated Temperature and Strain Rate Testing of Mg-Nb Multilayered Nanolaminates (**page 10**)
Extreme Temperature	2.2.1 Elevated Temperature Testing of Mg-Nb Multilayered Nanolaminates (**page 9**) 2.4 Structure, Properties and Performance of Solder Joints in Terrestrial vs. Reduced-Gravity Environments (**page 15**)

2.1.0 Engineering Metal-MAX Multilayered Nanocomposites (MMN): Hierarchical Microstructures for Tunable Strength and Toughness

Project Description: An integrated experimental and computational effort is in progress to engineer multilayered nanocomposite materials that exhibit unprecedented strength and toughness. The nanocomposite is composed of alternating metallic and MAX phase layers with a lamellar thickness reduced to the nanoscale. Unlike other multilayered systems, the metal-MAX materials detailed here are composed of a unique hierarchical topology – as interfaces between the layers are in direct competition with the internal interfaces within the MAX layers to drive the improved macroscopic mechanical behavior. Guided by experimental synthesis and novel nanomechanical testing capabilities, computational modeling will reveal the interfacial structures and stability at the atomic scale to elucidate the unique correlation of the hierarchical structure and mechanical properties – potentially offering additional avenues for property improvement through microstructural design.

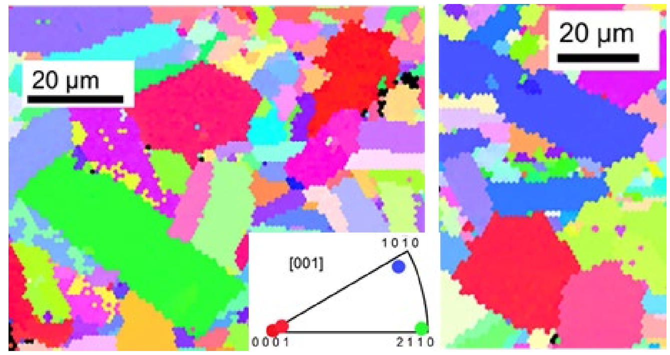

Fig 2. Electron backscattered diffraction maps of different areas on the Ta_2AlC sample. The inset IPF triangle indicates the selected orientations from both maps.

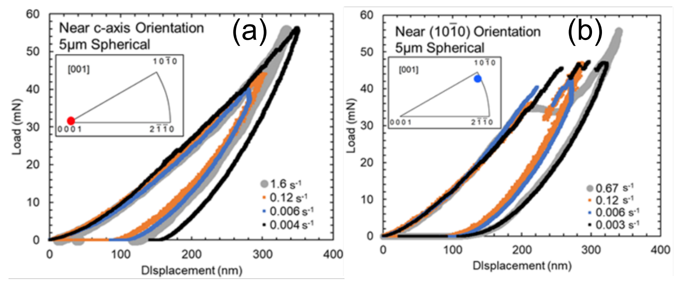

Fig 3. Load vs. displacement curves of nanoindentation at different strain rates using a 5 μm radius spherical tip on an orientation near parallel (a) and near perpendicular (b) to the basal orientation of Ta_2AlC.

2.1.1 High Strain Rate Response of Single Crystal MAX Phase Ta_2AlC

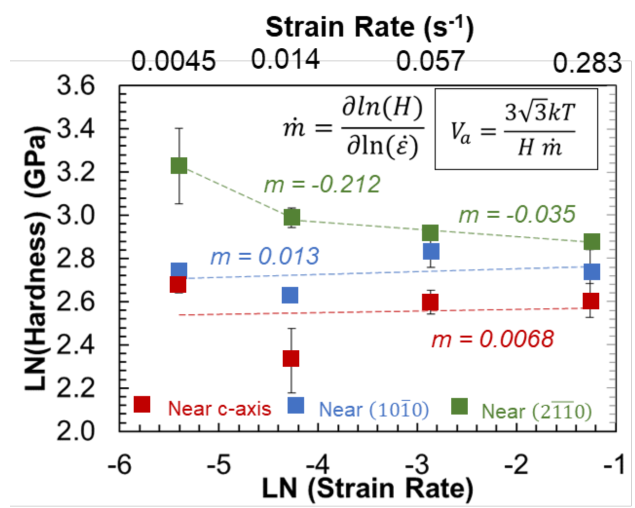

Orientation	Near c-axis	Near (10$\bar{1}$0)	Near (2$\bar{1}\bar{1}$0) (low s^{-1})	Near (2$\bar{1}\bar{1}$0) (high s^{-1})
Activation Volume (b^3)	19.92	8.55	-0.37	-2.71

Fig 4. (top) Plot of the hardness and strain rate normalized by LN on different orientations with associated strain rate sensitivity (m) values. (bottom) Tabulated calculated activation volumes based on burgers vector in a MAX phase Ta_2AlC.

To better understand deformation mechanisms and dislocation motion within MAX phases and provide experimental data to complement computational modeling, it is critical to understand the mechanical properties and behaviors of just MAX phases on different orientations. MAX phases are generally known to be anisotropic due to their atomically layered structure leading strains to be accommodated along the basal planes. In addition to anisotropy due to layering, MAX phases possess a hexagonal crystal structure which also often possess anisotropic properties. Specifically in this work, we focus on MAX phase Ta_2AlC with a calculated elastic anisotropy of 1.75, boasting the highest anisotropy factor among a group of M_2AlC where M = Ti, V, Cr, Nb, and Ta [5]. For that reason, MAX phase Ta_2AlC posed as a great candidate to perform micro- and nanomechanical testing using the expanded capabilities of the in-situ Alemnis nanoindenter on local regions to obtain single crystal responses from a polycrystalline sample.

With the expanded capabilities of the in-situ Alemnis nanoindenter, we utilize the high strain rate capabilities to determine the hardness at different strain rates and calculate the strain rate sensitivity (SRS). From the strain rate sensitivity, we can determine the activation volume [6] to understand and quantify volume associated with a single dislocation on the different orientations.

Polycrystalline Ta_2AlC was fabricated via hot pressing and was polished prior to EBSD mapping to find grain orientations large enough to perform several indents as well as being near parallel and perpendicular to the basal orientation (**Fig. 2**). Once the orientations are identified, we performed nanoindentation using the Alemnis nanoindenter from 0.0045 s^{-1} to 0.283 s^{-1} strain rates. Load vs. displacement curves on an orientation near parallel (**Fig. 3a**) and near perpendicular (**Fig. 3b**) to the basal orientation at the different strain rates show very different behaviors, with the orientation perpendicular to the basal orientation (**Fig. 3b**) showing drops in the load. We hypothesize that these drops are due to the atomic layers forming kinks due to being loaded parallel to the atomic layers. In contrast, we don't see these drops on the orientation near parallel to the basal orientation (**Fig. 3a**) – where the system is loaded perpendicular to the layers.

The strain rate sensitivity is subsequently calculated from the slope of a normalized hardness and strain rate (**Fig. 4a**), followed by calculations of the activation volume (**Fig. 4b**) [6, 7]. At most of the strain rates, the hardness was consistent. It is interesting to see a negative SRS. Moreover, we see a different behavior between the two orientations that are near perpendicular to the basal orientation (near $(10\bar{1}0)$ and near $(2\bar{1}\bar{1}0)$ orientations) suggesting a separate anisotropy between these orientations near perpendicular to the basal orientation. This is important to know as it will help guide the synthesis for engineering metal-MAX multilayered nanolaminates where we may try to promote the growth of a specific orientation over another depending on the desired material properties. Further testing at higher strain rates is in progress to better characterize the SRS on different orientations.

2.1.2 Stress-strain response of Ti-Ti_2AlC Multilayered deposited Metal and MAX phase nanocomposites and nanolaminates

To understand the deposition and fabrication of a metal-MAX phase multilayered nanolaminate system with a hierarchical layered structure, we chose to deposit a Ti-Ti_2AlC system. Titanium was chosen as the metal component 1) to improve co-deformation between the metal component in the MMN as well as the M layer within the MAX phase, 2) understand the effects of interdiffusion by having the metal component be the same as the M component in the MAX phase, and 3) to simplify the material system and better understand diffusion and dislocation behaviors of the MMN system.

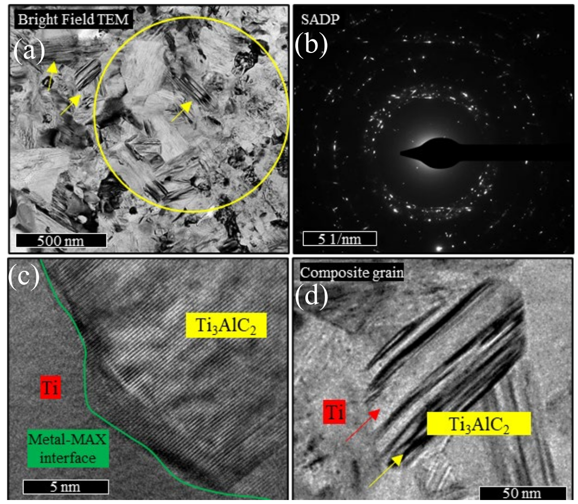

Fig 5. Bright field TEM (a) showing nanocrystalline grain structure with associated selective area diffraction pattern (SADP) (b). Region showing Ti and MAX Ti_3AlC_2 interface of nanocomposite (c) as well as Ti-Ti_3AlC_2 nanocomposite grain (d)

A first attempt of depositing the Ti-Ti_2AlC utilized physical vapor deposition (PVD) with a magnetron sputtering system at elevated temperatures of 800°C. Individual Ti, Al, and C targets were used, and the shutters were alternated between having all three shutters open and just the Ti shutter open for expitaxial growth on various Al_2O_3 and MgO substrate orientations. A film of ~ 4 µm was deposited and were preliminarily characterized using X-ray diffraction to confirm the presence of MAX phase Ti_2AlC and Ti in the deposition. Following confirmation of the presence of Ti and Ti_2AlC, further microstructure characterization was performed using TEM (**Fig. 5**). From conventional TEM studies, it was determined that the system possessed a nanocrystalline microstructure with areas of a Ti-Ti_2AlC nanocomposite grain structure. Furthermore, from precession electron diffraction (PED) mapping, we find the phase distribution and orientation of the local microstructure (**Fig. 6**). A high phase distribution of ~91% Ti_3AlC_2 is seen in the local region with a few regions of Ti_2AlC and Ti. We hypothesize that from the elevated temperature deposition (800°C is $0.48T_m$ for Ti and $0.267T_m$ for Ti_2AlC), there was enough thermal energy for the Ti layers to diffuse into the MAX phase Ti_2AlC and form nanocrystalline grains of Ti_3AlC_2.

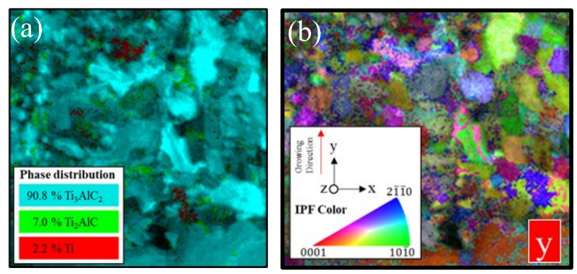

Fig 6. Precession electron diffraction map showing the phase distribution (a) and orientation (b) of Ti_3AlC_2 in a local region)

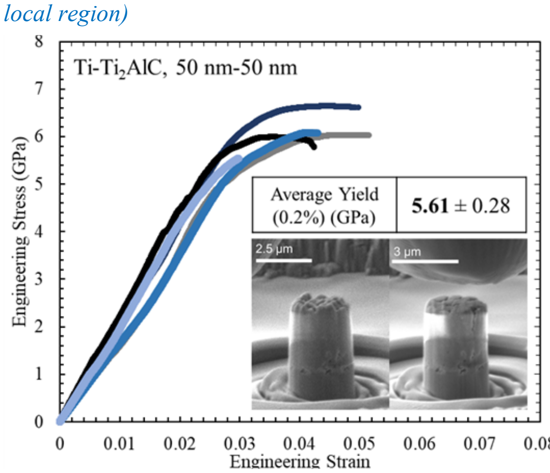

Fig 7. Stress-strain response of Ti-$Ti_{n+1}AlC_n$ nanocomposite. Inset shows pillar compression before and after compression before catastrophic failure.

In-situ micropillar compression was performed on this Ti-$Ti_{n+1}AlC_n$ nanocomposite system using the Alemnis nanoindenter. From micropillar compression (**Fig. 7**), the system demonstrated a high strength, yielding at 5.61 ± 0.28 GPa compared to those seen in Ti_3AlC_2 (around 105.7 – 441.8 MPa [8, 9]), and shortly after yield, the system fractured and failed catastrophically with little strain accommodation.

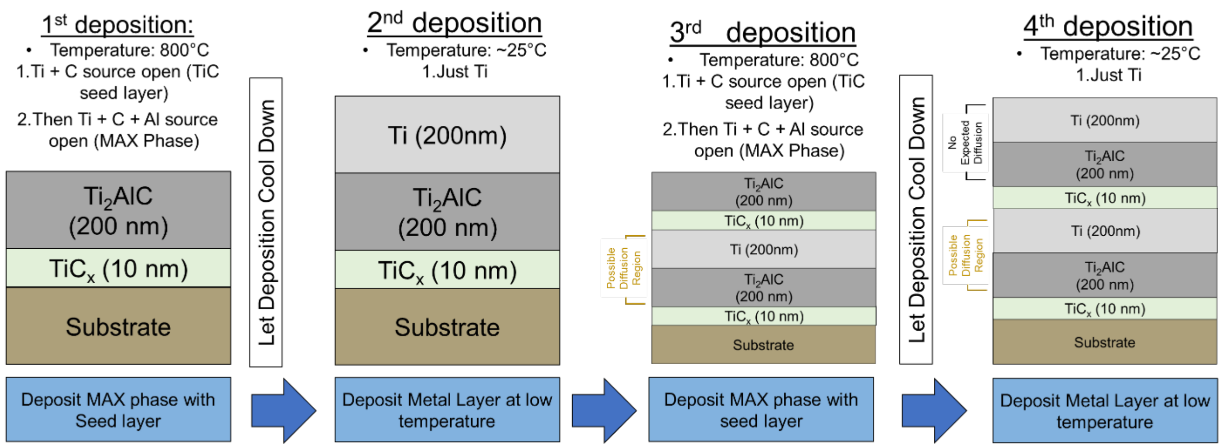

Fig 8. Schematic and process flow of the 4-step deposition of Ti-Ti2AlC system incorporating a TiC seed layer and deposition cooldown steps between the depositions to minimize diffusion.

Our second attempt involved two changes: the incorporation of a TiC seed layer to serve as a template and facilitate the growth of Ti_2AlC as well as the incorporation of a 4-step deposition process that involves cooldown step (**Fig. 8**) to minimize the amount of time the system is exposed to elevated temperature, thereby minimizing the extent of diffusion within the system. Additionally, we increased the layer thickness from an expected layer thickness of 30 nm to an expected layer thickness of 200 nm to investigate the extent of diffusion within the system. Like the previous deposition, preliminary investigations using XRD were performed to identify the presence of Ti and Ti_2AlC in the sample before proceeding to further microstructural and mechanical characterization. Strong peaks on the Al_2O_3 (0001) orientation prompted investigation on this sample.

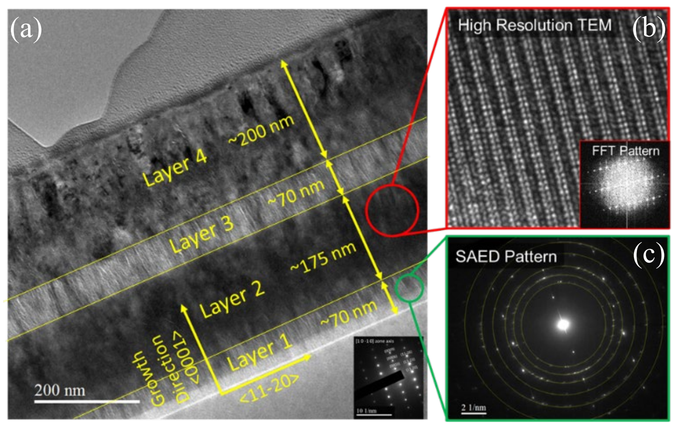

Fig 9. Bright-field TEM showing the microstructure of the film (a). High resolution TEM shows the signature lattice fringe structure for MAX phase (b), and SAED pattern shows the nanocrystalline nature of the film with slight texture (c).

Transmission electron microscopy investigations clearly indicate a multilayered deposition with distinct layers of what is expected to be Ti and Ti_2AlC (**Fig. 9**). High resolution TEM shows lattice fringes that are commonly associated with MAX phase structure (**Fig. 9b**). From the selective area electron diffraction (SAED) pattern (**Fig. 9c**), a nanocrystalline nature is observed with little to no texture within the film, and d-spacings matching with Ti and Ti_2AlC were identified. The different contrast in the 2nd layer compared with the 4th layer suggests that some diffusion may have occurred in the 2nd layer which is expected as this layer was briefly exposed to high temperatures in order to deposit the 2nd layer of TiC and Ti_2AlC MAX phase. Additionally, it is possible that the TiC may have served as a diffusion barrier between the 2nd and 3rd layer depositions as a sharp interface can be observed in the image. With these TEM investigations, we are the first to deposit a metal-MAX phase multilayered nanolaminate system.

Micropillar compression using the in-situ Alemnis nanoindenter was performed on this film following microstructural investigations (**Fig. 10**). A high strength is achieved with a yield of 2.86 ± 0.26 GPa compared to those for Ti_2AlC ranging from 0.039 GPa to 1 GPa [10]. Though the strength is lower than the previous deposition, the strain accommodation is greater than the previous deposition with an ultimate stress reached around 0.2 ± 0.1 ε compared to 0.04 ε. Three regions can also be identified within the stress-strain plot, consisting of an initial yield, most likely of the softer metal Ti layers, followed by a second yield, with when the MAX phase also begins to yield, and ending with slight strain hardening with a complete plastic flow within the system. Furthermore, no catastrophic failure was observed in any micropillar. The high strain accommodation may be attributed to the large layers of Ti within the system. The high strength is most likely attributed to the nanocrystalline nature within the individual layers. Further microstructural characterization involving TEM and STEM coupled with energy dispersive spectroscopy (EDS) of undeformed and deformed micropillars will be performed to confirm the chemical composition of the system and better understand the deformation mechanisms and mechanical behavior of the system.

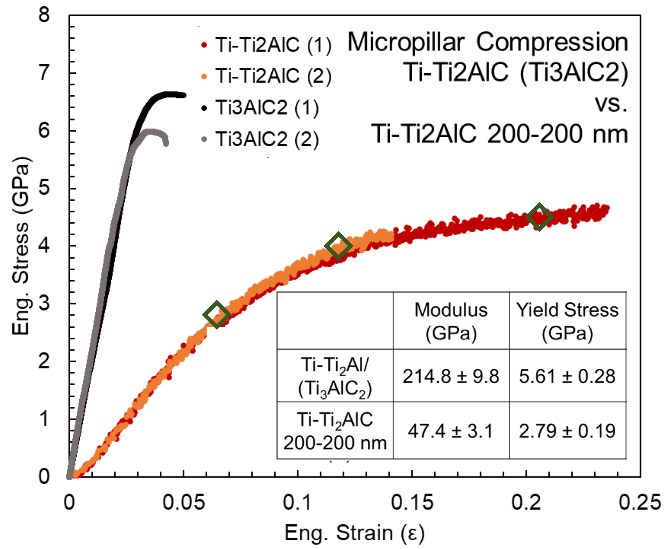

Fig 10. *Stress-strain plot comparing the two Ti-Ti_2AlC deposited nanocomposite and nanolaminate systems. Square indicators represent breakpoints for the different regions in the curves*

From these two depositions, the true displacement control nature of the in-situ Alemnis nanoindenter was critical to observe the deformation behavior and compare the mechanical properties of the two systems.

2.2.0 Simultaneous high strength and mechanical stability of pseudomorphic bcc Nb/Mg nanolaminates

Project Description: While bimetallic nanocomposites have demonstrated extraordinary – three to even ten-fold – gains in strength with decreasing layer thickness, their strengths tend to plateau beyond a critical layer thickness. More disappointingly, such increases in strength are almost always accompanied by a decrease in their strains to failure (ductility) [11, 12]. In our previous works [13], including experiments conducted at APS [14], we have reported simultaneous improvements in <u>*both*</u> strength and mechanical stability of Nb/Mg nanolaminates with decreasing layer thicknesses, a trend seldom reported in nanolaminates consisting of pure metals. This unique observation was explained by a pseudomorphic phase transformation in Mg, where at low enough layer thicknesses (<7-8 nm) the crystal structure of Mg in Mg/Nb nanolaminates can be transformed and stabilized from simple hexagonal (hcp) to a more ductile body center cubic (bcc) at ambient pressures through interface strain engineering (Fig. 1) [15]. Using micro-pillar compression and nanoindentation experiments we showed that physical vapor deposited (PVD) Mg/Nb nanolaminates that contain a bcc Mg pseudomorphic phase demonstrate a >60% increase in strength and a >80% increase in strain to failure over those containing the hcp Mg phase [13]. Instead of a strength plateau, the hcp-to-bcc phase transition in Mg results in a renewed strengthening regime in the nanolaminate caused by the change to a coherent interface from an incoherent one, along with a concurrent increase in strain-to-failure due to the introduction of a more plastically isotropic bcc material from an anisotropic hcp structure [16]. This method provides a radical approach to overcoming the strength and ductility problem in traditional hexagonal close-packed (hcp) Mg.

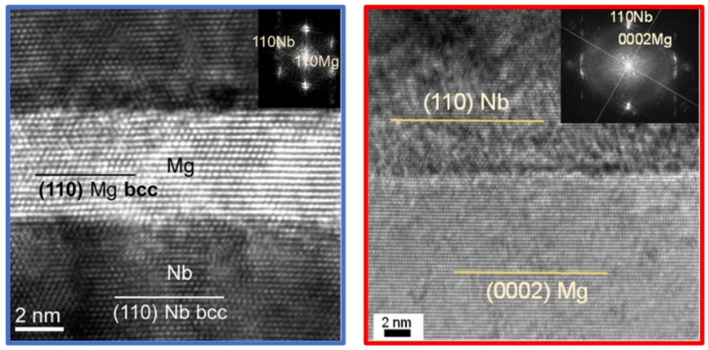

Fig 11. High resolution TEM images of the 5.5 – 5.5 nm Mg-Nb multilayer (a) and 35 – 35 nm Mg-Nb multilayers. Insets represents the associated FFT.

With the Alemnis nanoindenter system, we aim to investigate the operative deformation mechanisms of pseudomorphic bcc Mg under both ambient and extreme conditions of temperature, pressure, and strain rates.

2.2.1 Elevated Temperature Testing of Mg-Nb Multilayered Nanolaminates

We utilize magnetron sputtering PVD to fabricate two sets of Mg and Nb multilayers: one set with individual layer thicknesses of 5.5 nm, and another set with individual layer thicknesses of 35 nm. Through prior analytical and DFT calculations, it is suggested that BCC mg phase can be maintained up to a critical value of 4.2 nm from the interface. For a

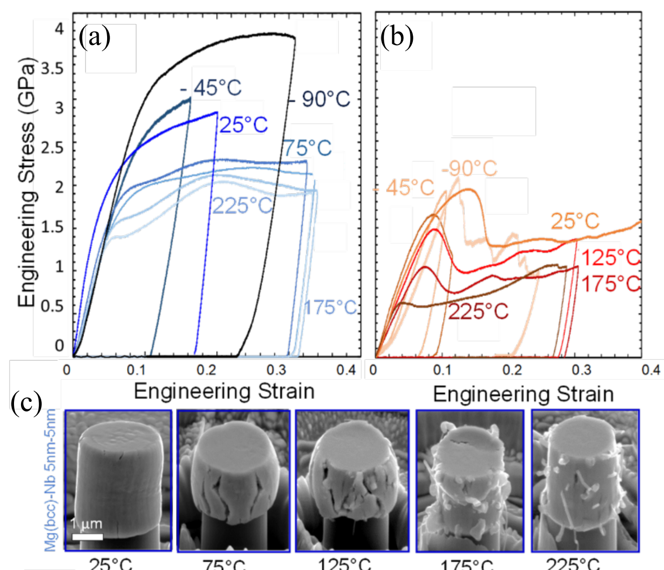

Fig 12. Micropillar compression of 5.5 – 5.5 nm Mg-Nb multilayers (a) and 35 – 35 nm Mg-Nb multilayers (b) at low and elevated temperatures. SEM micrographs of the post deformation of the micropillar of the 5.5 – 5.5 nm Mg-Nb multilayer at v low and elevated temperatures (c)

nanolayered composite this corresponds to a critical Mg layer thickness of ~8.4 nm; thus, one deposited system is below and another is above the critical layer thickness. Microstructure characterization was performed using XRD, X-ray synchrotron (XRS) measurements, as well as TEM. From XRD and XRS measurements the presence of BCC Mg was seen in the 5.5 nm deposition, and the lattice parameter of BCC mg was 3.347 Å which is similar to that for Nb which is 3.304 Å. For the 35 nm deposition, consistent 35 nm layers with HCP Mg was identified. From the bright field TEM and corresponding diffraction pattern we observe that both phases are highly textured. High resolution TEM images confirm the BCC crystal structure in Mg (**Fig. 11**) and as well as confirm the coherent interface between the Mg and Nb layers.

To complement the microstructure investigations, mechanical property characterization was performed using the in-situ Alemnis nanoindenter. We performed low temperature and elevated temperature micropillar compression at -90°C, -45°C, 25°C, 75°C, , 125°C, 175°C, and 225°C on both the 5.5 – 5.5 nm and 35 – 35 nm depositions (**Fig. 12**). From the stress-strain plots, the Mg (HCP) – Nb (BCC) multilayers show an instability upon reaching peak stress, whereas the Mg (BCC) – Nb (BCC) multilayers maintain its stability and do not show any large drops in stress. In both cases, the yield stress increases with decreasing temperatures. From the micrographs, we see a change in strain accommodation mechanisms, with large cracks forming at the low temperatures, while at high temperatures it appears that material – most likely Mg from the lighter contrast – is being expunged out.

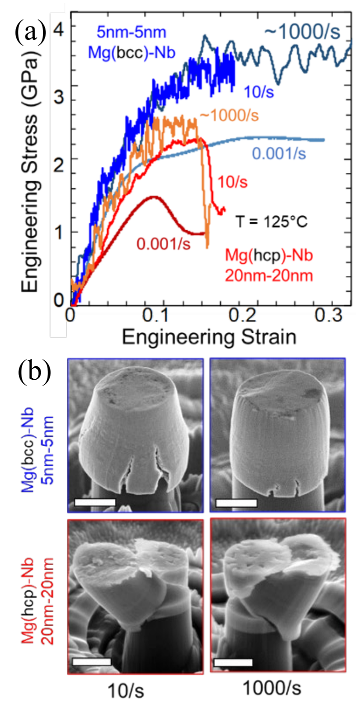

Fig 13. (a) Micropillar compression of 5 – 5 nm Mg-Nb multilayers and 20 – 20 nm Mg-Nb multilayers low to high strain rates at elevated temperatures of 125°C. (b) SEM micrographs of post deformed micropillars

2.2.2 Combined Elevated Temperature and Strain Rate Testing of Mg-Nb Multilayered Nanolaminates

In addition to the thermal stability of Mg-Nb multilayers, we utilize the in-situ Alemnis nanoindenter with its ability to combine high strain rate indentation with low to elevated temperatures. Tests were performed at quasi-static strain rates (0.001 s^{-1} and 0.01 s^{-1}) to high strain rates (10 s^{-1} and 1000 s^{-1}) at room temperature (25°C) and elevated temperatures at 125°C (**Fig. 13a**) on both a 5 – 5 nm Mg (BCC) – Nb (BCC) and 20 – 20 nm Mg (HCP) – Nb (BCC) multilayered nanolaminates. An increase in strain hardening can be seen with increasing strain rates in both systems, and an instability can be seen upon reaching peak stress in all cases of the 20 – 20 nm Mg (HCP) – Nb (BCC) system at the various strain rates. In comparison the 5 – 5 nm system does not show any pronounced stress instability. This may be due to the higher strength associated with the BCC crystal structure of Mg and the reduced layer thickness leading to possible confined layer slip (CLS) strengthening [16-18]. SEM micrographs of post deformed micropillars show very different deformation between the two systems (**Fig. 13b**). Slip dominated deformation is seen in the 20 – 20 nm Mg-Nb multilayered system, while crack formation and propagation is seen in the 5 – 5 nm Mg-Nb multilayered system. The crack dominated response may be due to the reduced layer thickness and the deformation associated with CLS.

From the yield stress at different strain rates, it is possible to calculate a strain rate sensitivity (m). In addition, this SRS can be calculated and used to determine the activation volume for dislocations at elevated temperatures (**Fig. 14a**). From the SRS plot at different temperatures, it can be seen that a much smaller volume is associated with the 5 – 5 nm Mg-Nb multilayers and there is little change in the activation volume compared to the larger 20 – 20 nm Mg-Nb multilayers. This is most likely linked to the crystal structure, suggesting that BCC Mg is less sensitive to changes in temperature. It is also possible to use the SRS with yield stress at various temperatures to determine the activation energy for dislocation motion (**Fig. 14b**)

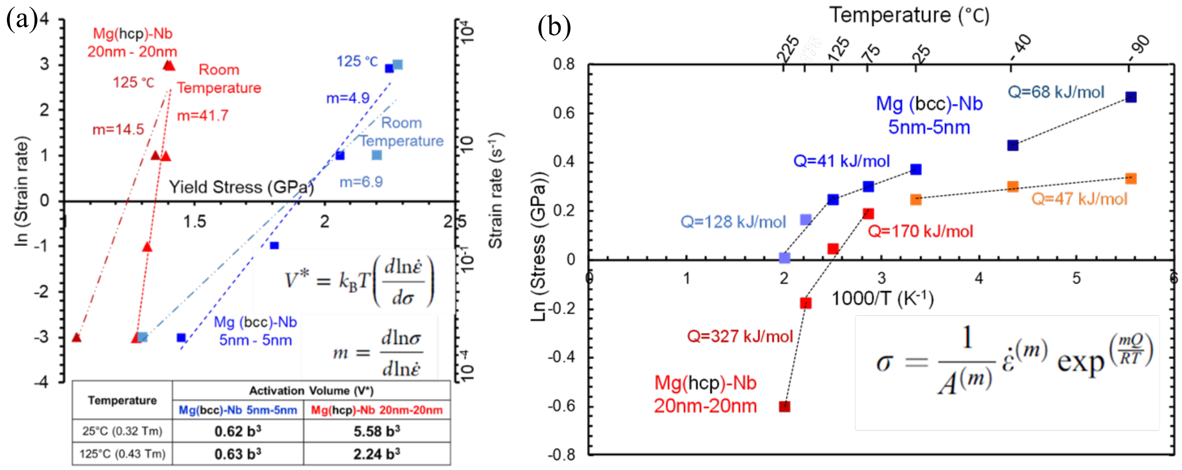

Fig 14. Normalized strain rate vs yield stress plot with calculated SRS values at room temperature and elevated temperatures of 125°C (a). Normalized yield stress vs. normalized inverse temperature plot with determined the activation energy values (b)

[13, 19, 20]. A lower change in activation energy is observed to be associated with the 5 – 5 nm Mg-Nb multilayers further suggesting a lower sensitivity to temperature. Furthermore, there is a higher activation energy associated with the 20 – 20 nm Mg-Nb multilayers at higher temperatures suggesting that it is more sensitive to changes in temperatures. In all cases, we find that the 5 – 5 nm Mg-Nb multilayers possess higher strength at various temperatures and strain rates. Normally, it is difficult to experimentally determine the activation energy and activation volume for new material systems, however with the extended capabilities of the in-situ Alemnis nanoindenter, it becomes more feasible to investigate such properties.

2.2.3 Micro-Tension-Compression Asymmetry in Mg-Nb Multilayered Nanolaminates

For a comprehensive study of the Mg-Nb multilayered nanolaminate system, we investigate the micro-tension-compression asymmetry using micropillar compression and microtensile tension using specially fabricated tensile grippers. Micropillars were fabricated and tested parallel to the layer interfaces (**Fig. 15**) in both compression and tension. In microcompression, a higher yield stress, modulus, and strain accommodation is observed in the 5.5 – 5.5 nm Mg-Nb multilayers compared to the larger 18.9 – 14.1 nm Mg-Nb multilayer. This is perhaps due to the increased strength of a reduced layer thickness from CLS strengthening. In microtension, yield and catastrophic failure occurred shortly after yield in both cases. From TEM investigations (**Fig. 16**), a waviness can be observed in the layers, forming columnar boundaries. Nanopores can be found at these columnar boundaries. We hypothesize that these nanopores are an artifact of the magnetron sputtering PVD. The presence of these nanopores within the deposition is especially detrimental when subjected to tensile loading which may be the source of the similar failure seen in both Mg-Nb layer thicknesses. The slightly higher tensile yield stress and modulus is observed in the 5.5 – 5.5 nm Mg-Nb multilayer, possibly due to the CLS strengthening.

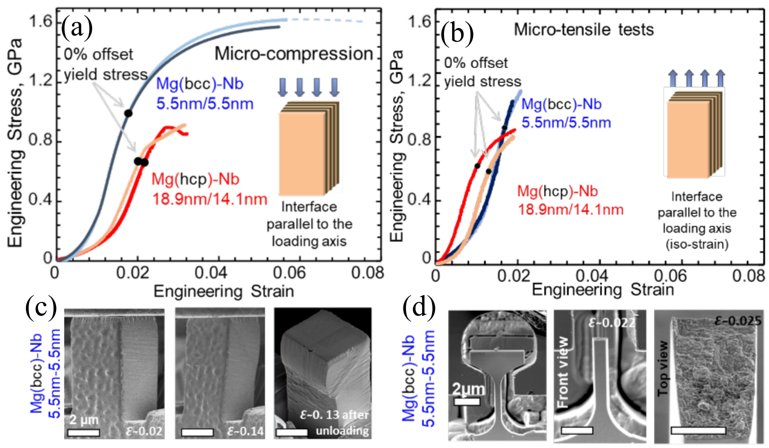

Fig 15. *Stress-strain plots in microcompression (a) and microtension (b) of the 5.5 – 5.5 nm Mg-Nb and 18.9 – 14.1 nm Mg-Nb multilayers with insets showing the loading schematic of the layers. SEM micrographs of the 5.5 – 5.5 nm Mg-Nb multilayers at various strains during microcompression (c) and microtension (d)*

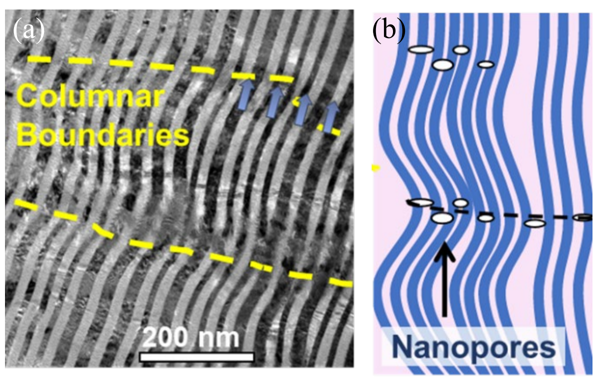

Fig 16. *Bright field TEM of the 18.9 – 14.1 nm Mg-Nb multilayers (a) showing waviness and columnar boundaries. A schematic showing nanopores associated with the columnar boundaries (b)*

2.3 Fracture Studies of Cu-TiN and Al-TiN Multilayered Nanolaminates using Microcompression

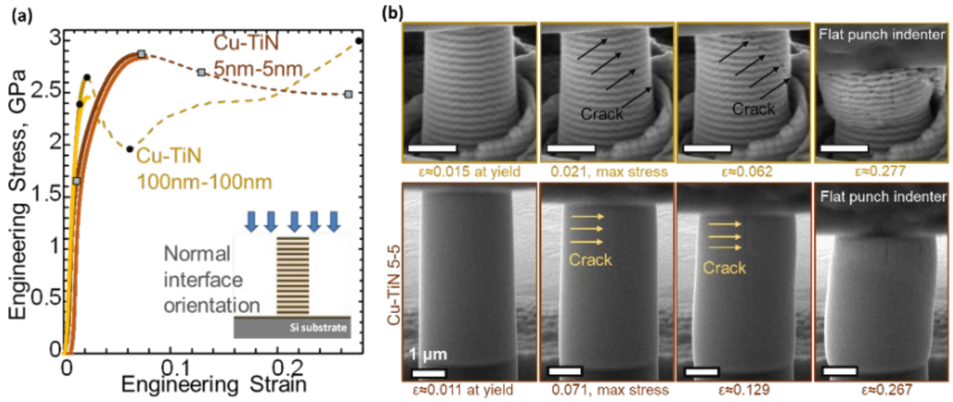

Fig 17. (a) Stress-strain response of Cu(100nm)-TiN(100nm) and Cu(5nm)-TiN (5nm) multilayer nanolaminate in normal (Normal interface orientation) loading conditions. (b) SEM micrograph of pillars showing the deformation at different strain levels.

We performed in-situ SEM micropillar compression to study the fracture in physical vapor deposited Cu-TiN multilayered nanolaminates. Micropillars were fabricated using the focused ion beam and were tested using the in-situ SEM nanoindenter. In micro-compression testing, 100nm-100nm Cu-TiN multilayer nanolaminates in normal and parallel interface orientation show higher yield strength than the 5nm-5nm Cu-TiN (**Figs. 17a and 18a**). Previous studies have shown that Cu-TiN nanolaminate exhibit weak dependence on the layer thickness and is better correlated to the grain size [12]. In normal interface orientation, the crack propagation in the 100nm-100nm Cu-TiN is at 45º to the loading direction (**Fig. 17b**) whereas, it is in the loading direction in 5nm-5nm Cu-TiN nanolaminate (**Fig.17b**). In parallel interface orientation, 100nm-100nm Cu-TiN nanolaminate shows crack propagation at 45º to the loading direction (**Fig 18b**) whereas, 5nm-5nm Cu-TiN nanolaminate shows material shear off at 45º to the loading direction (**Fig 18b**). For the 45º inclined interface orientation in 50nm-50nm Cu-TiN, higher yield strength is observed for pillar A than for pillars B and C (**Fig 19a**). However, 5nm-5nm Cu-TiN in 45º inclined interface orientation shows similar strength as 50nm-50nm Cu-TiN pillar A in the same orientation (**Fig 19a**). Pillar A shows crack formation and layer parallel sliding, whereas pillar C shows crack propagation at 45º to the applied load. The 5nm-5nm Cu-TiN pillar 1 in 45º inclined interface orientation shows layer parallel sliding.

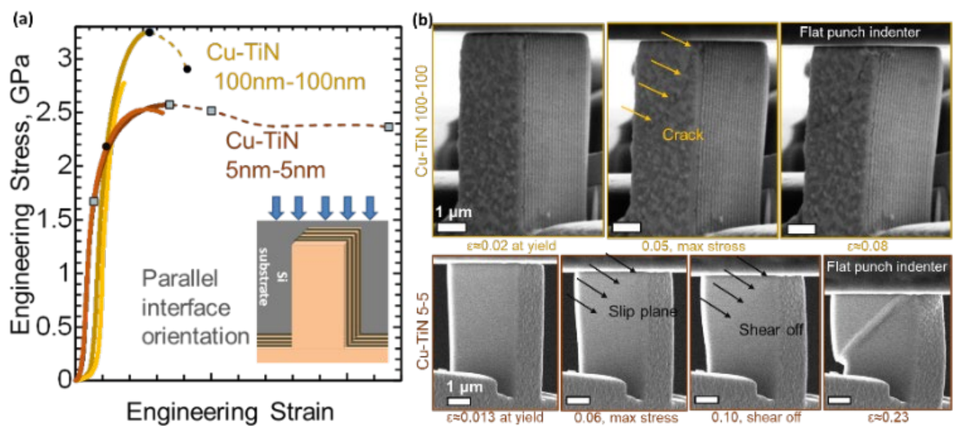

Fig 18. (a) Stress-strain response of Cu(100nm)-TiN(100nm) and Cu(5nm)-TiN (5nm) multilayer nanolaminate in parallel (parallel interface orientation) loading conditions. (b) SEM micrograph of pillars showing the deformation at different strain levels.

We also performed in-Situ SEM micropillar compression to study the fracture in physical vapor deposited Al-TiN multilayered nanolaminates. In micro-compression testing, 5nm-5nm Al-TiN multilayer nanolaminates in normal, parallel and 45º inclined interface orientation show higher yield strength and lower plasticity than the 50nm-50nm Al-TiN which may be attributed to the lower layer thickness (**Fig. 20a, 20c, 21a**). In normal interface orientation Al-TiN nanolaminate, cracks can be seen at the max stress where they propagate at 45º to the loading direction, followed by catastrophic failure (**Fig. 20b**). In parallel interface orientation, 50nm-50nm Al-TiN nanolaminate, cracks are observed to propagate in the direction of the loading. In contrast, they are seen to propagate at 45º to the loading direction in 5nm-5m Al-TiN. Both the 5nm-5nm and 50nm-50nm Al-TiN shows layer parallel sliding in 45º inclined interface orientation. In case of Al-TiN, Parallel interface orientation shows higher yield strength than the normal and 45º inclined interface orientation.

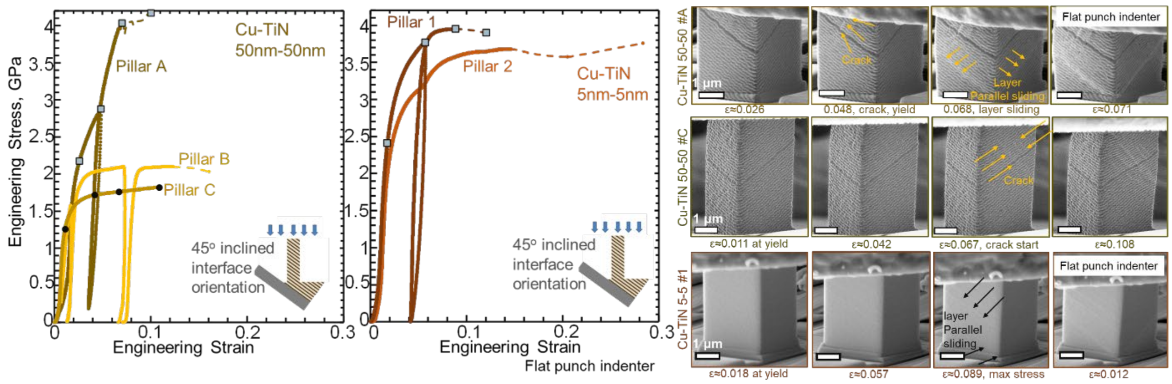

Fig 19. (a) Stress-strain response of Cu(100nm)-TiN(100nm) and Cu(5nm)-TiN (5nm) multilayer nanolaminate in 45º (45º inclined interface orientation) loading conditions. (b) SEM micrograph of pillars showing the deformation at different strain levels.

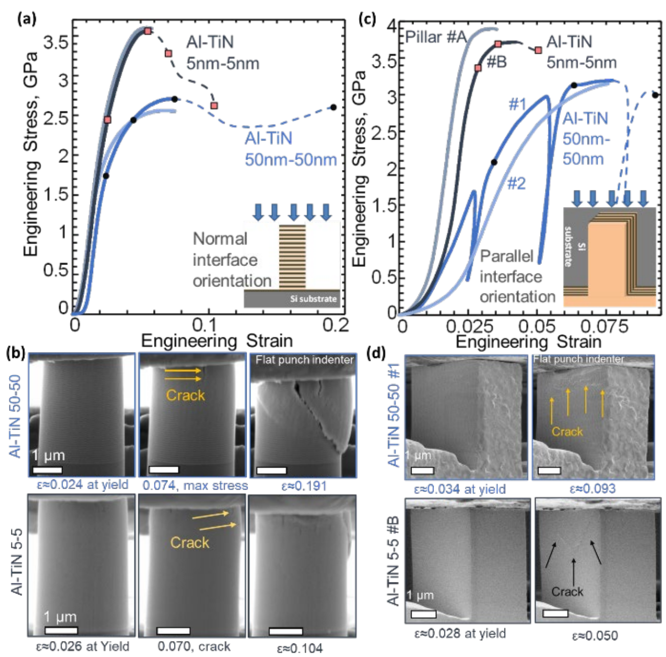

Fig 20. (a, c) Stress-strain response of Al(50nm)-TiN(50nm) and Al(5nm)-TiN (5nm) multilayer nanolaminate in normal (normal interface orientation) and parallel (parallel interface orientation) loading conditions, respectively (b,d) SEM micrograph of pillars in normal and parallel interface orientation, respectively, showing the deformation at different strain levels.

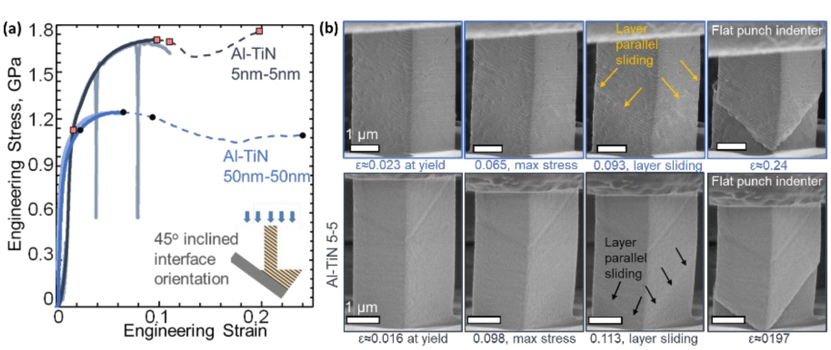

Fig 21. (a) Stress-strain response of Al(50nm)-TiN(50nm) and Al(5nm)-TiN (5nm) multilayer nanolaminate in 45º (45º inclined interface orientation) loading conditions (b) SEM micrograph of pillars showing the deformation at different strain levels.

2.4 Structure, Properties and Performance of Solder Joints in Terrestrial vs. Reduced-Gravity Environments

Scientific/Technical Summary: This investigation combines experiments and modeling to elucidate the fundamental mechanisms, phenomenology, and process conditions that govern the integrity and performance of solder joints produced in terrestrial vs. reduced gravity environments, such as the microgravity conditions onboard the International Space Station (ISS). We utilize solder samples from the In-Space Soldering Investigation (ISSI) experiments from the Physical Sciences Informatics (PSI) repository [21, 22], as well as expand into other non-ISSI solder compositions, and combine space- and ground-based experiments with advanced 3D materials characterization, micromechanical testing, and mesoscale modeling. In particular, the project addresses the formation and persistence of porosity through the reflow/filling/freezing processes and the deleterious effects on microstructure and mechanical properties of the solder joint. It has been established [21, 22] that porosity arising from flux volatilization, which is dispersed and expelled from the solder joint under terrestrial gravity, may become entrapped within the freezing solder material under microgravity conditions, given the absence of buoyancy-driven convection. Our overall goals are (i) to advance the current qualitative understanding of this phenomenon into the realm of alloy/process-specific quantitative description and prediction and (ii) to examine the effects of mechanically and acoustically stimulated flow while assessing their potential effectiveness as porosity mitigation strategies for solder-based fabrication processes in space. Considering a range of potential applications and materials, 3 solder alloys will be investigated, including the ISSI lead-based (Pb-Sn) solders, as well as lead-free (Sn-Ag-Cu and Sn-Au) solders, which have recently shown promise for high-performance joint applications due to their good thermal, electrical conductivities and excellent corrosion, fatigue resistance [23-25]. The understanding gained in this study will enable robust and reliable protocols for solder-based solutions to address repair and fabrication needs for long-duration human exploration missions in (and beyond) low Earth orbit (ex: Moon, Mars).

Background and Motivation: An effective solder alloy will readily wet the substrate components and spontaneously flow into tight crevices under the action of capillary forces. The non-destructive nature of the soldering process - with only short-time exposure to moderate temperatures and no melting or dissolution of the components themselves – promotes applicability to a wide range of fabrication and repair scenarios, both manual and automated. Indeed, lead-based (e.g. Pb-Sn) and lead-free (e.g. Sn-Ag-Cu) solders are ubiquitous in electrical, electronic, structural, container, and flow/pipe applications. Proven as a flexible and robust process suitable for joining many (even dissimilar) materials, soldering is a potential solution to a variety of *in-space* fabrication needs, including (i) in-flight repairs of electrical/electronic devices, plumbing systems, and structural/mechanical components and (ii) sealing/resealing rigid containers with high structural/environmental integrity for long-term protective storage or transport. The prospect of reliable *in-space* soldering under microgravity conditions, however, presents numerous challenges, and space-flight experience is limited to a small number of in-service component repairs [26]. Experimental reports are also few but demonstrate important differences between ground and space conditions. Most importantly, experiments on sounding rockets, parabolic flights, and low-earth-orbit have shown the following points (**Fig. 22**).

- Reduced buoyancy-driven convection in space promotes the entrapment of flux and a corresponding increase in internal porosity arising from flux volatilization [26, 27]
- Flux/pore entrapment is deleterious to performance (e.g. 32% shear strength decrease associated with 14% porosity increase in Sn-Ag-Cu, comparing parabolic flight joints to ground-based [28].)
- Flux entrapment is strongly influenced by flux application and heating processes.
- Thermocapillary flow becomes dominant in the absence of buoyance-driven convection, demonstrating the importance of joint configuration and control of process conditions [21, 22, 29]

The present proposed work builds on a recently concluded NASA PSI grant (#80NSSC20K0223, PI – S Pathak) that aimed to characterize both the microstructure and resultant micro-to-nano mechanical response of solders in terrestrial vs. microgravity environments, 1g vs 10^{-5}g, from the original ISSI study led by NASA Scientist Dr. Richard Grugel [21, 22]. The ISSI experimental procedure consisted of 84 soldering experiments conducted on the ISS in 2003-04, and an equivalent set of ground-based experiments using identical equipment and supplies. The ground-based experiments involved conductively melting 10 cm lengths of 40Pb-60Sn (3.3 wt% rosin/flux) solder onto a loop turned into the silver coated copper wire. On Earth, tests showed the solder melting sagging, dropping, or running down the test wire due to buoyancy (density) effect. During this process, the entrapped gases and the water vapor evolving from the circuit board itself are transported to the joint surface and mostly eliminated while the joint is molten (**Fig. 22a, c**). In comparison, aboard the ISS the molten solder was observed to form an equilibrium "football" shape (**Fig. 22b**). The changes in geometric shape are believed to be due to the dominance of surface tension in microgravity (**Fig.22a,b**). There are many different susceptible defects in soldering operations such as gas bubbles and voids (**Fig.22c,d**). The solder samples prepared aboard the ISS exhibited a considerable amount of internal porosity (about seven times that of ground-based solders), as shown in the scanning electron microscope (SEM) micrographs in Figs. 1c vs. d. The 3-D microstructural information from non-destructive micro-computed tomography (micro-CT) demonstrates the 3-D distribution of voids in the microgravity solder (**Fig. 23**). The increased porosity

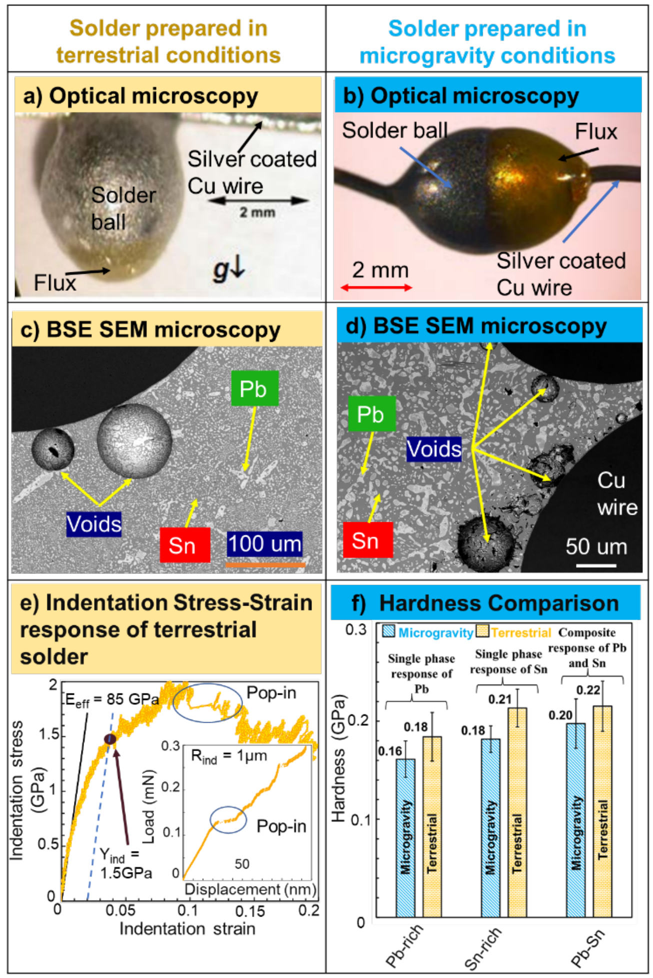

Fig. 22. Comparison of the structure and properties of terrestrial vs. microgravity Pb-Sn solders using (a, b) optical microscopy vs. (c, d), backscattered electron (BSE) maps and (e, f) local property information using indentation analysis.

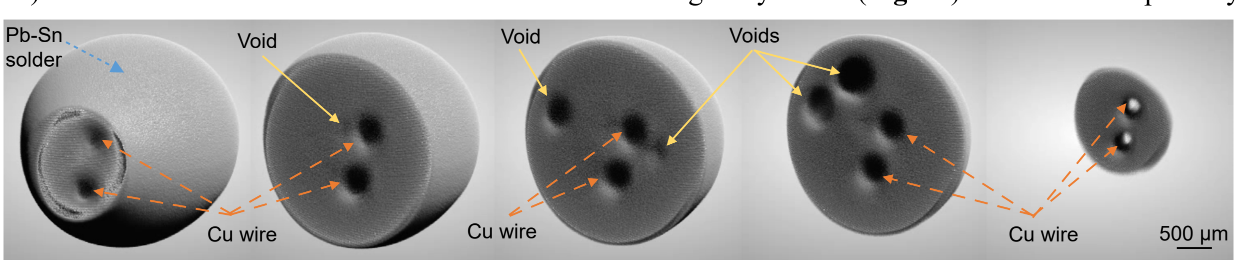

Fig 23. 3-D distribution of voids in microgravity Pb-Sn solder using micro-computed tomography.

is believed to be due to the lack of buoyant forces on flux and water vapor inherently present in the molten solder. Entrapped gases will remain within the molten pool of solder until the solidification is complete, resulting in higher amounts of voids and compromising the mechanical integrity and electrical properties of the joint. Our current results also show a distinct difference of the distribution of the Sn-rich and Pb-rich regions (**Figs. 22c vs. 22d**) of the terrestrial vs. microgravity solders using electron backscatter imaging and a lower strength in the microgravity solders from nanoindentation testing (**Figs. 22e, f**).

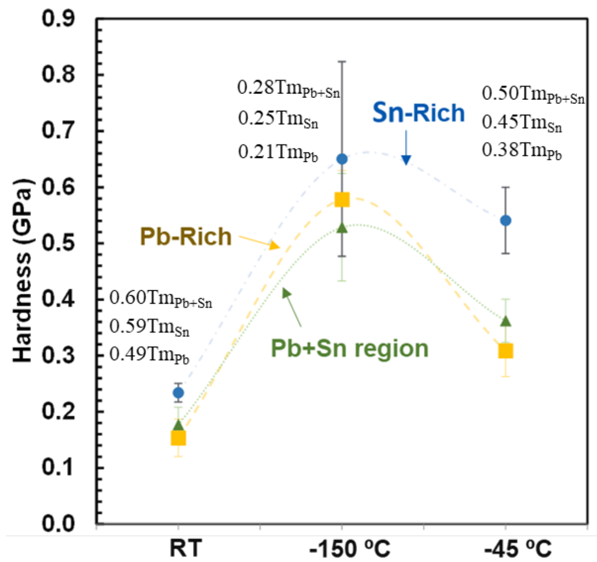

Fig 24. *Hardness response from Pb-rich phase, Sn-rich phase and Pb+Sn regions obtained from in-Situ SEM nanomechanical testing at RT, -45ºC, -150ºC. Hardness from different regions increases with decreasing the temperature below the room temperature.*

The use of the in-Situ SEM Alemnis nanoindenter provides the advantage of evaluating the materials in extreme environments. For space applications, materials are subjected to ultracold temperature, and it is important to understand the mechanical performance of the electronic components at extreme temperatures. We studied the micro-mechanical behavior of the solder joints under extreme conditions of elevated and cryogenic temperatures similar to those typically experienced by the ISS (from +120ºC on sun-facing side to -150ºC on shady side outside the ISS). These tests examine the effects of ductile to brittle transition, allotropic phase transformation, and associated volume and internal stress changes in Sn in Pb-Sn solders during the β-Sn (body-centered tetragonal) to α-Sn (diamond cubic) transformation below 13ºC. We performed Berkovich indentation using in-situ SEM Alemnis nanoindenter on the terrestrial solder sample. We observed that the hardness response from the Pb-rich phase, Sn-rich phase, and Pb+Sn regions increases with a decrease in temperature (**Fig. 24**). The hardness response from Pb+Sn regions is lower than the individual phase at room temperature and -45ºC, but it lies between the hardness response of the individual phase at -150ºC. This change in the hardness response of the Pb+Sn regions may be associated with interface behavior as interfaces play an important role when we indent deeper into the material to get a bulk response. The increased solder hardness at -45ºC is probably associated with the lack of thermal assistance (lower than the RT and higher than -150ºC) in the dislocation motion and formation of less dense α-Sn. Post-cryo-SEM imaging also shows possible nucleation of α-Sn at the surface (Fig. 20). The increased solder hardness at -150ºC (higher than -45ºC and RT) is probably associated with multiple factors: 1) There is a lack of thermal assistance in the dislocation motion (lower than -45ºC and RT) 2) High-stress concentration due to the deformation twinning below DBTT temperature (-125ºC).

2.5 Micromechanical Investigations of the Remarkable Damage Tolerance in Tooth-Enamel of Hadrosaurid Dinosaurs

The principal objective of this research is to understand the biomechanical form, function, and structure of the enamel (a ceramic-like composite) known as aprismatic coarse wavy enamel (CWE) in the grinding dentition of large herbivores hadrosaurid dinosaurs. Our preliminary analysis of this tissue shows an undulating wavy structure in WE composed of folded layers of hydroxyapatite crystallites separated by thin layers of loosely aggregated interlayer matrix. This study specifically focuses on how the undulating wavy structure of this enamel helped dinosaurs' teeth to deflect cracks and provided the exceptional strength and toughness to mitigate the effects of fracture promoting sediments while masticating.

A set of experimental tasks involving microstructure characterization and small-scale mechanical testing techniques were proposed to achieve the following principal objectives: For microstructural characterization we used optical microscopy (surface topography), scanning electron microscopy (SEM) (surface morphology), Raman spectroscopy (molecular fingerprint) and atom probe tomography (atomic scale composition). This was correlated with the small-scale testing techniques like spherical nanoindentation (sub µm to 10s of µm volume- achieved by changing indenter radius) and more specialized in-situ micropillar compression testing (few µm to 10s of µm volume – achieved by changing pillar dimensions). These tests were performed for: a) Individual layers probing local response and b) for bulk CWE probing global response. The structure property relationship showed the most prominent effect of elastic mismatch present among the individual layers and the undulating wavy interfaces in influencing the damage tolerance behavior of CWE. Furthermore, the findings of this study were employed to develop a bio inspired damage tolerant metal-ceramic metal ceramic nanocomposite laminate with elastic mismatch and a degree of undulating interfaces present among the alternating metal ceramic layers. The fracture experiments revealed similar crack deflection behavior as seen in CWE. The knowledge gained from this thesis research will be advantageous in 1) Applied materials sciences: the field of multilayer composites where alternating layers of stiff vs. compliant material along with the introduction of waviness among the layers (similar to WE structure) has showed improved crack deflection abilities and 2) Evolutionary biology and paleontology, where understanding gained from this research can be applied to more complex

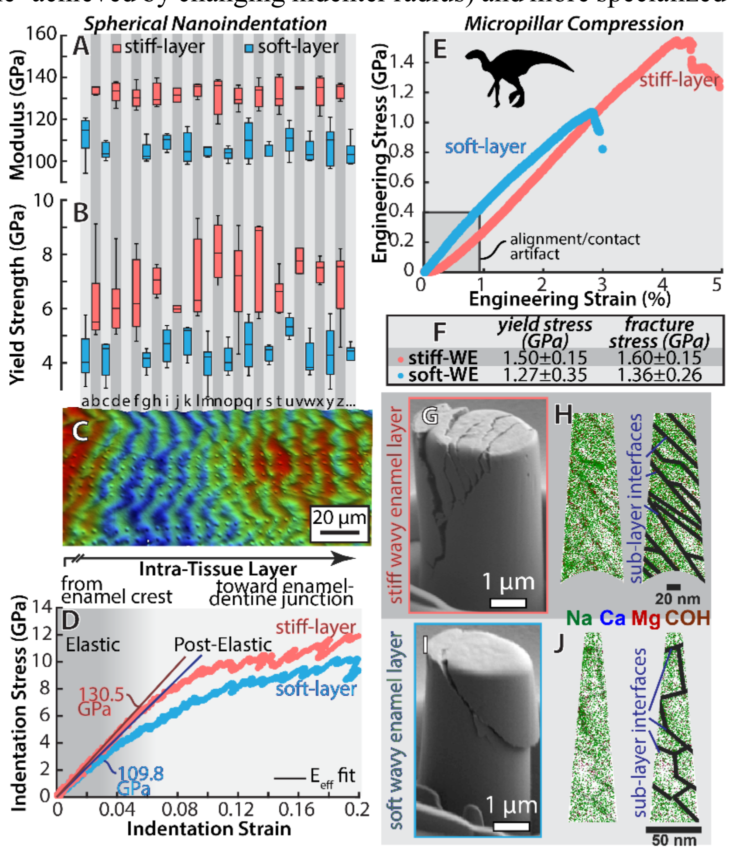

Fig 25. Combined structure-property maps of (A) elastic (modulus) and (B) plastic (indentation yield strength) of WE. (C) Optical profilometry of WE. (D) Representative indentation stress-strain responses from alternating harder (stiffer) and softer WE tissue layers. (E, F, G, I) Fracture response of harder and softer tissue layers of WE using in-situ SEM micro-compression testing. (H, J) APT results from harder and softer WE layers showing sub-layer interfaces.

grinding dentition like modified radial enamel (MRE) found in the grinding dentition of horses, bovids, suids etc., and irregular enamel found in mammoths and elephants.

Hadrosaurids, unlike mammals with grinding dentitions utilized undulating CWE (= folded layers of parallel hydroxyapatite crystallites separated by thin layers of loosely aggregated inter-layer matrix, **Fig. 25C**), the most complex enamel known in any reptilian taxon [30]. CWE has a highly complex hierarchical internal structure and is a particularly challenging material to characterize mechanically, especially at the micron length scales where the mineral and voids once occupied by collagen components are closely intertwined and the available testing methods are limited. We utilized the high-throughput of the indentation stress-strain technique to demonstrate correlations between the elastic/plastic mechanical properties of CWE to the corresponding structural (topographical) information measured using optical profilometry at similar μm length scales. **Figs. 25A, B and D** show that the trends of both the elastic (indentation modulus) and plastic (yield strength) properties are highly complementary to each other and closely reflect the 2D optical profilometry map of the harder and softer enamel tissue layers shown in **Fig. 25C**. The structure-property maps in **Figs. 25A and B** reflect the unique morphology of the CWE layering, where the periodic variations in properties between the layers, combined with the enamel layer undulations, is postulated to promote the remarkable fracture resistance, localized damage and strategically controlled crack directionality of this structure. These results demonstrate the applicability of combined structure-indentation studies on mineralized dental tissues,

Micro-mechanical Test Strategies enabled by the Alemnis indenter system. In addition to indentation, research using the Alemnis indenter also focused on developing novel techniques for nano to micro-scale compression, tensile and fracture toughness testing. At these length scales, focused ion beam (FIB) milling processes are highly efficient in micro-fabrication of nanomechanical test structures from a bulk sample [31, 32] such as cylindrical micro-scale compression samples (**Figs. 25E-J**), dog bone geometries for micro-tensile testing [33-35], as well as three-point bend and cantilever bend samples techniques [33-35]. A myriad of mechanical property information, such as elastic modulus (E), yield strength (σ_y), flow stress (σ_f), strain hardening co-efficient (n), fracture toughness (K_c) etc., can be obtained through mechanical testing of such miniaturized test structures which can probe small volumes of material of the order of 1 μm^3 or smaller. Extension of these techniques to the CWE tissue shows clear differences between the fracture behavior under compression of the harder (higher yield and fracture strength) vs. softer tissue layers in hadrosaurid CWE (**Figs. 25G-J**). Intriguingly, the harder tissue layers show initiation of multiple cracks before fracture (**Fig. 25G**), suggesting another level of hierarchy where this layer could be composed of weaker interfaces and subsequent sub-layers. APT results (**Figs. 25H, J**) confirm the above hypothesis. Such insights are crucial for effective approaches to biomimetic designs originating from the CWE structure.

Inspiration for bio-mimetic design. Our research also explored the possibility of extending the natural biological design of CWE towards the development of new synthetic (wavy) layered composites, which are comprised of metallic or ceramic constituents with individual layer thicknesses ranging from millimeters down to less than a few nanometers [36-40]. Metal/ceramic multilayers [12] are especially attractive due to

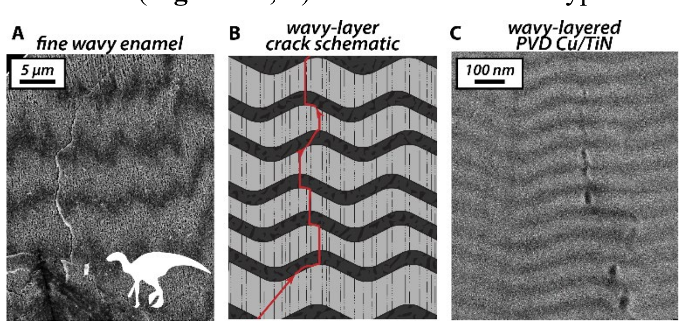

***Fig 26**. (A) Experimental results and (B) schematic of crack deflection in hadrosaurid WE, which inspired our (C) PVD deposited wavy 50nm-50nm metal-ceramic Cu-TiN multilayers. showing crack undulation (strain energy loss) and controlled-crack propagation along the waviness between the layers.*

the large differences in strength and ductility between their constituent phases (**Fig. 26, and earlier Figs 17-21**), and these property contrasts constitute the simplest form of model heterogeneous materials [41] for ductile phase toughening of brittle materials [42, 43]. Using the knowledge gained from the dinosaur CWE, the PI team incorporated the undulating architecture of the hadrosaurid wavy enamel (WE, see **Figs. 25C and 26A**) on to a 50nm-50nm Cu-TiN multilayered nanolaminate structure, synthesized using physical vapor deposition techniques (**PVD, Fig. 26C**). Such enamel layer undulations in hadrosaurids are known to localize damage and strategically control crack directionality (**Fig. 26B**). Note how the addition of the waviness to the layering of the metal-ceramic multilayer (**Fig. 26C**) is similarly instrumental in undulating the crack propagation, thus robbing the crack tip of the required strain energy and controlling its propagation through the laminate.

3.0 Impact on Research-Related Education and Training Infrastructure

Both the PI and Iowa State University have taken various steps to foster materials science related educational activities, with recent emphasis on courses that involve cross-cutting disciplines, such as biology and materials science. The following undergraduate and graduate classes are regular users of the existing characterization facilities at MSE-ISU, and have incorporated the Alemnis indenter into their coursework.

***Table 2**: Teaching Activities Related to the Alemnis Indenter System*

Course (Undergraduate)
MAT E 418 Mechanical Behavior of Materials
MAT E 456 BioMaterials
MAT E 413/4 Materials Senior Design

The Senior Design course (MAT E 413/414) deserves special mention. ISU-MSE senior design projects are required in order to obtain an undergraduate degree from the College of Engineering at ISU. The projects are 6 credits divided over two semesters (Fall-Spring, or Spring-Fall).The PI is very active with senior design projects, and the award-winning 2018-19 senior design team from his previous position at UNR has already worked on a design project based on the Alemnis system. The PI is already in discussion with the industry partner for this project - Alemnis AG – for involvement in a follow-up design project by providing resources and guidance to a materials undergraduate student team. Additionally, a significant utilization of this instrument is expected from the **Ames National Laboratory** user base (note: Ames Lab is an US DoE national laboratory affiliated with and located on the ISU campus where the PI has an affiliated status).

Installation and Interface with Existing Facilities and Equipment, Maintenance and Operation: The DURIP **f**unds were dispersed in early January 2021, with the purchase order of the extended capabilities and system shortly placed in February 2021. After the purchase order was received the system was processed and prepared by Alemnis AG and shipped to ISU by the end of July 2021. Installation and user training took place in November 2021 with Skye Supakul, Soumya Varma, Manish Jain, and PI Sid Pathak learning the standard system, the ultra-high strain rate system, the cryo system, and the ultra-high temperature system. A new-user instruction guide has been prepared by the trained students and will serve as a starting point for training new students. The main graduate students from the PI's group are currently responsible for the operation, maintenance and management of the equipment. The included 1-year warranty in the price of the equipment is facilitating uninterrupted usage and help in the management of the instrument.

Operating the Alemnis platform inside the SEM provides seamless access to the EBSD, EDS, and FIB (along with regular electron microscopy imaging) without having to break vacuum, thus maximizing the productive time spent on the microscope and as well as protecting sensitive samples from atmospheric exposure between tests. As mentioned earlier the Alemnis platform is small, compact, and portable, and thus can be moved between labs/buildings. Hence the Alemnis SEM Indenter can be mounted easily to any of the two SEM systems available at MSE-ISU (the FEI Quanta 250 Field Emission SEM, JEOL SEM). Additionally, ISU and Ames Laboratory have together acquired and installed state-of-the-art materials characterization equipment in the *Sensitive Instrument Facility (SIF)*. There are two SEMs available at the SIF at Ames National Lab (FEI Helios NanoLab G3 UC (Ultimate Characterization) Dual-Beam SEM/FIB, and the FEI Teneo Low Vacuum FE-SEM). Of these four instruments the FEI Teneo is currently the primary 'home' for the Alemnis SEM Indenter due to its additional FIB, EBSD and EDS capabilities, although the Almenis indenter can be operated on all four SEMs at MSE-ISU and Ames.

References

[1] J.M. Wheeler, C. Harvey, N. Li, A. Misra, N.A. Mara, X. Maeder, J. Michler, S. Pathak, High temperature nanoindentation of Cu–TiN nanolaminates, Materials Science and Engineering: A (2020) 140522.
[2] M. Rouhani, F. Chau-Nan Hong, Y.-R. Jeng, In-situ thermal stability analysis of amorphous carbon films with different sp3 content, Carbon 130 (2018) 401-409.
[3] K. Wasmer, T. Wermelinger, A. Bidiville, R. Spolenak, J. Michler, In situ compression tests on micron-sized silicon pillars by Raman microscopy—Stress measurements and deformation analysis, Journal of Materials Research 23(11) (2011) 3040-3047.
[4] R. Ghisleni†, J. Liu†, R. Raghavan, P. Brodard, A. Lugstein, K. Wasmer, J. Michler, In situ micro-Raman compression: characterization of plasticity and fracture in GaAs, Philosophical Magazine 91(7-9) (2011) 1286-1292.
[5] Z. Sun, S. Li, R. Ahuja, J.M. Schneider, Calculated elastic properties of M2AlC (M=Ti, V, Cr, Nb and Ta), Solid State Communications 129(9) (2004) 589-592.
[6] V. Maier, K. Durst, J. Mueller, B. Backes, H.W. Höppel, M. Göken, Nanoindentation strain-rate jump tests for determining the local strain-rate sensitivity in nanocrystalline Ni and ultrafine-grained Al, Journal of Materials Research 26(11) (2011) 1421-1430.
[7] J.M. Wheeler, V. Maier, K. Durst, M. Göken, J. Michler, Activation parameters for deformation of ultrafine-grained aluminium as determined by indentation strain rate jumps at elevated temperature, Materials Science and Engineering: A 585 (2013) 108-113.
[8] E. Drouelle, A. Joulain, J. Cormier, V. Gauthier-Brunet, P. Villechaise, S. Dubois, P. Sallot, Deformation mechanisms during high temperature tensile creep of Ti3AlC2 MAX phase, Journal of Alloys and Compounds 693 (2017) 622-630.
[9] Z. Zhan, M. Radovic, A. Srivastava, On the non-classical crystallographic slip in Tin+1AlCn MAX phases, Scripta Materialia 194 (2021) 113698.
[10] Z. Zhan, Y. Chen, M. Radovic, A. Srivastava, Non-classical crystallographic slip in a ternary carbide – Ti2AlC, Materials Research Letters 8(7) (2020) 275-281.
[11] A. Misra, J.P. Hirth, R.G. Hoagland, Length-scale-dependent deformation mechanisms in incoherent metallic multilayered composites, Acta Materialia 53(18) (2005) 4817-4824.
[12] S. Pathak, N. Li, X. Maeder, R.G. Hoagland, J.K. Baldwin, J. Michler, A. Misra, J. Wang, N.A. Mara, On the origins of hardness of Cu–TiN nanolayered composites, Scripta Materialia 109 (2015) 48-51.
[13] S. Pathak, N. Velisavljevic, J.K. Baldwin, M. Jain, S. Zheng, N.A. Mara, I.J. Beyerlein, Strong, Ductile, and Thermally Stable bcc-Mg Nanolaminates, Scientific Reports 7(1) (2017) 8264.
[14] M. Jain, N. Velisavljevic, J.K. Baldwin, M. Knezevic, N.A. Mara, I.J. Beyerlein, S. Pathak, Structure and properties of pseudomorphically transformed bcc Mg in Mg/Nb multilayered nanolaminates studied using synchrotron X-ray diffraction, Journal of Applied Physics 126(2) (2019) 025302.
[15] B. Ham, X. Zhang, High strength Mg/Nb nanolayer composites, Materials Science and Engineering: A 528(4–5) (2011) 2028-2033.
[16] M. Ardeljan, M. Knezevic, M. Jain, S. Pathak, A. Kumar, N. Li, N.A. Mara, J.K. Baldwin, I.J. Beyerlein, Room temperature deformation mechanisms of Mg/Nb nanolayered composites, Journal of Materials Research 33(10) (2018) 1311-1332.
[17] N. Li, J. Wang, A. Misra, J.Y. Huang, Direct Observations of Confined Layer Slip in Cu/Nb Multilayers, Microscopy and Microanalysis 18(5) (2012) 1155-1162.
[18] J. Wang, M. Knezevic, M. Jain, S. Pathak, I.J. Beyerlein, Role of interface-affected dislocation motion on the strength of Mg/Nb nanolayered composites inferred by dual-mode confined layer slip crystal plasticity, Journal of the Mechanics and Physics of Solids 152 (2021) 104421.
[19] G. Mohanty, J.M. Wheeler, R. Raghavan, J. Wehrs, M. Hasegawa, S. Mischler, L. Philippe, J. Michler, Elevated temperature, strain rate jump microcompression of nanocrystalline nickel, Philosophical Magazine 95(16-18) (2014) 1878-1895.

[20] J.M. Wheeler, L. Thilly, A. Morel, A.A. Taylor, A. Montagne, R. Ghisleni, J. Michler, The plasticity of indium antimonide: Insights from variable temperature, strain rate jump micro-compression testing, Acta Materialia 106 (2016) 283-289.
[21] R. Grugel, D. Gillies, L. Murphy, J.A. Ogle, G. Funkhouser, F. Parris, A.V. Anilkumar, F. Hua, Final Research Report. In-Space Soldering Investigation (ISSI), 2006.
[22] R.N. Grugel, P. Luz, G. Smith, R. Spivey, L. Jeter, D. Gillies, F. Hua, A.V. Anilkumar, Materials research conducted aboard the International Space Station: Facilities overview, operational procedures, and experimental outcomes, Acta Astronautica 62(8) (2008) 491-498.
[23] P.J. Wang, J.S. Kim, C.C. Lee, Fluxless Bonding of Large Silicon Chips to Ceramic Packages Using Electroplated Eutectic Au/Sn/Au Structures, Journal of Electronic Materials 38(10) (2009) 2106-2111.
[24] B.-S. Lee, C.-W. Lee, J.-W. Yoon, Comparative study of Au–Sn and Sn–Ag–Cu as die-attach materials for power electronics applications, Surface and Interface Analysis 48(7) (2016) 493-497.
[25] J. Xu, M. Wu, J. Pu, S. Xue, Novel Au-Based Solder Alloys: A Potential Answer for Electrical Packaging Problem, Advances in Materials Science and Engineering 2020 (2020) 4969647.
[26] J.K. Watson, P.M. Struk, R.D. Pettegrew, R.S. Downs, Experimental Investigation of Solder Joint Defect Formation and Mitigation in Reduced-Gravity Environments, AIAA Journal of Spacecraft and Rockets 44(1) (2007) 174-182.
[27] C.A. Winter, J.C. Jones, The Microgravity Research Experiments (MICREX) Data Base, NASA Technical Memorandum NASA TM-108523, 1996.
[28] B. Thomas, A. Atkinson, R.J. Dashwood, Strength of Soldered Joints Formed under Microgravity Conditions, Journal of Electronic Materials 36(1) (2007) 1-5.
[29] R.N. Grugel, D.C. Gillies, F. Hua, A. Anilkumar, The In-Space Soldering Investigation: To Date Analysis of Experiments Conducted on the International Space Station, 2006 National Space and Missile Materials Symposium, Orlando, FL, 2006.
[30] G.M. Erickson, B.A. Krick, M. Hamilton, G.R. Bourne, M.A. Norell, E. Lilleodden, W.G. Sawyer, Complex dental structure and wear biomechanics in hadrosaurid dinosaurs, Science (New York, N.Y.) 338(6103) (2012) 98.
[31] A. Kunz, S. Pathak, J.R. Greer, Size effects in Al nanopillars: Single crystalline vs. bicrystalline, Acta Materialia 59(11) (2011) 4416-4424.
[32] M.D. Uchic, D.M. Dimiduk, J.N. Florando, W.D. Nix, Sample dimensions influence strength and crystal plasticity, Science 305(5686) (2004) 986-989.
[33] K.J. Hollis, N.A. Mara, R.D. Field, T.A. Wynn, J.M. Crapps, P.O. Dickerson, Bond Characterization of Plasma Sprayed Zirconium on Uranium Alloy by Microcantilever Testing, J Therm Spray Tech 22(2-3) (2013) 233-241.
[34] B.N. Jaya, C. Kirchlechner, G. Dehm, Can microscale fracture tests provide reliable fracture toughness values? A case study in silicon, Journal of Materials Research 30(5) (2015) 686-698.
[35] S. Zheng, I.J. Beyerlein, J.S. Carpenter, K. Kang, J. Wang, W. Han, N.A. Mara, High-strength and thermally stable bulk nanolayered composites due to twin-induced interfaces, Nature Communications 4 (2013) 1696.
[36] N. Mara, I. Beyerlein, Review: effect of bimetal interface structure on the mechanical behavior of Cu–Nb fcc–bcc nanolayered composites, J Mater Sci 49(19) (2014) 6497-6516.
[37] I.J. Beyerlein, N.A. Mara, J.S. Carpenter, T. Nizolek, W.M. Mook, T.A. Wynn, R.J. McCabe, J.R. Mayeur, K. Kang, S. Zheng, J. Wang, T.M. Pollock, Interface-driven microstructure development and ultra high strength of bulk nanostructured Cu-Nb multilayers fabricated by severe plastic deformation, Journal of Materials Research 28(13) (2013) 1799-1812.
[38] S.J. Zheng, I.J. Beyerlein, J. Wang, J.S. Carpenter, W.Z. Han, N.A. Mara, Deformation twinning mechanisms from bimetal interfaces as revealed by in situ straining in the TEM, Acta Materialia 60(16) (2012) 5858-5866.
[39] N.A. Mara, I.J. Beyerlein, J.S. Carpenter, J. Wang, Interfacially Driven Deformation Twinning in Bulk Ag-Cu Composites, JOM 64(10) (2012) 1218-1226.

[40] N. Li, N.A. Mara, J. Wang, P. Dickerson, J.Y. Huang, A. Misra, Ex situ and in situ measurements of the shear strength of interfaces in metallic multilayers, Scripta Materialia 67(5) (2012) 479-482.
[41] C.J. Hsueh, L. Avellar, B. Bourdin, G. Ravichandran, K. Bhattacharya, Stress fluctuation, crack renucleation and toughening in layered materials, Journal of the Mechanics and Physics of Solids 120 (2018) 68-78.
[42] E. Munch, M.E. Launey, D.H. Alsem, E. Saiz, A.P. Tomsia, R.O. Ritchie, Tough, Bio-Inspired Hybrid Materials, Science 322(5907) (2008) 1516.
[43] M.E. Launey, E. Munch, D.H. Alsem, E. Saiz, A.P. Tomsia, R.O. Ritchie, A novel biomimetic approach to the design of high-performance ceramic-metal composites, J R Soc Interface 7(46) (2010) 741-753.